


Article

On Fractional Discrete Memristive Model with Incommensurate Orders: Symmetry, Asymmetry, Hidden Chaos and Control Approaches

Hussein Al-Taani ¹ , Ma'mon Abu Hammad ², Mohammad Abudayah ¹, Louiza Diabi ^{3,*} and Adel Ouannas ⁴

¹ School of Electrical Engineering and Information Technology, German Jordanian University, Amman 11180, Jordan; hussein.taani@gju.edu.jo (H.A.-T.); mohammad.abudayah@gju.edu.jo (M.A.)

² Department of Mathematics, Al-Zaytoonah University of Jordan, Amman 11733, Jordan; m.abuhammad@zuj.edu.jo

³ Laboratory of Dynamical Systems and Control, University of Larbi Ben M'hidi, Oum El Bouaghi 04000, Algeria

⁴ Department of Mathematics and Computer Sciences, University of Larbi Ben M'hidi, Oum El Bouaghi 04000, Algeria; ouannas.adel@univ-oeb.dz

* Correspondence: louiza.diabi@univ-oeb.dz

Abstract: Memristives provide a high degree of non-linearity to the model. This property has led to many studies focusing on developing memristive models to provide more non-linearity. This article studies a novel fractional discrete memristive system with incommensurate orders using θ_i -th Caputo-like operator. Bifurcation, phase portraits and the computation of the maximum Lyapunov Exponent (LE_{max}) are used to demonstrate their impact on the system's dynamics. Furthermore, we employ the sample entropy approach (SampEn), C_0 complexity and the 0-1 test to quantify complexity and validate chaos in the incommensurate system. Studies indicate that the discrete memristive system with incommensurate fractional orders manifests diverse dynamical behaviors, including hidden chaos, symmetry, and asymmetry attractors, which are influenced by the incommensurate derivative values. Moreover, a 2D non-linear controller is presented to stabilize and synchronize the novel system. The work results are provided by numerical simulation obtained using MATLAB R2024a codes.

Keywords: incommensurate order; sigmoidal function; chaos; complexity; control



Academic Editors: Chunbiao Li, Eric Campos-Cantón, Sen Zhang, Tengfei Lei and Xudong Gao

Received: 4 December 2024

Revised: 15 January 2025

Accepted: 17 January 2025

Published: 18 January 2025

Citation: Al-Taani, H.; Abu Hammad, M.; Abudayah, M.; Diabi, L.; Ouannas, A. On Fractional Discrete Memristive Model with Incommensurate Orders: Symmetry, Asymmetry, Hidden Chaos and Control Approaches. *Symmetry* **2025**, *17*, 143. <https://doi.org/10.3390/sym17010143>

Copyright: © 2025 by the authors. Licensee MDPI, Basel, Switzerland. This article is an open access article distributed under the terms and conditions of the Creative Commons Attribution (CC BY) license (<https://creativecommons.org/licenses/by/4.0/>).

1. Introduction

Memristive-based discrete mathematical models have been studied because they are quick, flexible, easy to implement and computationally efficient [1]. The concept behind these integer-order discrete models is memristors, which stand for non-linear circuit components associated with the linkage of magnetic flux and electric charge [2]. The appearance of chaos in discrete memristor models has also been studied. There are a certain chaotic map-based memristive models in [3–5]. The observation of various chaotic behaviors thus suggests that the memristive parameters have an impact on the system's complexity.

Discrete fractional models have shown to be more accurate at explaining complex non-linear phenomena than conventional continuous fractional systems [6,7]. Fractional calculus has proven to be more accurate than traditional integer-order calculus at describing complex non-linear phenomena, exhibiting their special qualities such as flexibility, viscosity and long-term memory [8]. This accuracy and adaptability highlight the growing interest in using fractional calculus to analyze contemporary, complex systems. However,

fractional calculus offers improved tools to comprehend system dynamics over time and offers deeper insights into chaotic behavior and stability in dynamical systems. In particular, discrete fractional calculus has garnered superb attention in light of its potential to handle fractional derivatives, compared with classical fractional calculus, which focuses on integer-order difference operators. Many domains have seen its application, such as data encryption, physics, chemistry and biology [9]. More specifically, in the literature appears to be a noticeable lack on the study of dynamic systems under incommensurate-order derivatives. Owing to this, the study and research in this field grant the special qualities and advantages of incommensurate fractional systems [10]. It has been discovered in recent years that models with incommensurate orders are more flexible. The incommensurate fractional derivative is actually a particular instance of fractional-order systems wherein the orders have distinct values. This distinction from homogeneous fractional orders gives the dynamics of the system an additional level of complexity and adaptability, enabling more in-depth investigation of its characteristics [11,12]. Namely, in reference [11], Hamadneh et al. discussed the dynamics of a novel sine-based memristor map with commensurate and incommensurate fractional orders, while in [12] the authors control chaotic behavior in a new map under incommensurate fractional order.

In recent years, a crucial discipline for research is the exploration of chaotic dynamics in discrete fractional non-linear models expressed by discrete difference equations. Despite their simple structures, chaotic systems can display complex behavior, which lends chaos theory a broad and multidisciplinary application [13]. For accurate modeling and prediction of the behavior of complex systems, it is essential to identify and comprehend hidden chaos because it emphasizes the significance of taking into account potential tipping points that could cause a transition from stable to chaotic. Hidden attractors are crucial for understanding complex system behaviors because they can arise in stable systems as well and cause unanticipated dynamics like sudden chaos. An attractor that is not connected to any equilibrium points in a dynamical system is known as a hidden attractor, and it is difficult to find using conventional methods. Its detection necessitates particular techniques and well-chosen initial conditions. Hidden chaos denotes a condition of underlying disorder or unpredictability that is not always evident but may become apparent in specific circumstances and is important in many disciplines [14]. In contrast to normal chaos, which is obvious in systems that behave erratically and unpredictably, it can appear when a system encounters particular disturbances. For instance, in [15], the authors studied the chaotic attractors of a different fractional memristor-based discrete system, while Wu et al. analyzed the behaviors of a hidden chaotic fractional systems in [16]. As a result, several control techniques and synchronization have been suggested to stabilize various discrete fractional chaotic systems [17]. The chaotic behavior of the system can be managed using a variety of control strategies, according to earlier research. To ensure that the chaotic dynamics stay within the intended bounds, the oscillation magnitudes are specifically controlled by amplitude control. Furthermore, the system's baseline is modified using displacement boosting, which shifts the balance to meet the particular operational requirements. Furthermore, it is possible for the system to evolve with little intervention under free control and under complete control, which governs the entire system's transition between chaotic and normal phases. A thorough framework for efficiently controlling the dynamics of the system is offered by these control strategies [18]. Overall, a great deal of research has been conducted on the stabilization of chaotic systems in the literature. It describes how a chaotic system can be adaptively controlled to drive its states to zero over time. Our research has been motivated by the fact that, as far as we are aware, there are no such studies for fractional-order chaotic maps. Synchronization, a process that uses adaptive control parameters to make a slave system follow the same trajectory as a master,

is another significant feature of chaotic systems [19–21]. For example, in [19], control and synchronization of a 4D fractional chaotic map with constant and variable order were studied. Moreover, stabilization and synchronization of fractional chaotic discrete-time models was explored in [20], whereas in [21] synchronization of fractional hidden chaotic discrete-time models was developed.

In the study of chaos theory, symmetry and asymmetry are important concepts that affect the behavior and evolution of chaotic systems, and a system's stability under specific transformations is referred to as symmetry. Moreover, symmetric structures can result in stable behaviors and predictable patterns in chaotic systems. But even small perturbations that cause this symmetry to break can bring about big changes, resulting in behavior that is chaotic and unpredictable [22,23]. On the other hand, asymmetry indicates the absence of this stability, which is frequently a sign of chaotic systems. Small disturbances have the potential to amplify and cause unpredictable behavior in asymmetric systems. The way that symmetry and asymmetry interact in chaos is crucial to comprehending how orderly states give way to chaotic ones. It is possible to predict and even control chaotic behavior by understanding how symmetry breaking can result in chaos. Recently, there have been many manuscripts published on the symmetric. For example, Ref. [24] proposes a new method of digital communication built on a coherent chaotic data transmission strategy, while [25] analyzes symmetry chaotic fractional maps and their rich dynamics. In contrast, some attention has been dedicated of to the asymmetric. In [26], the asymmetric memristive jerk circuit's coexisting bifurcation and multistability were examined. Reference [27] investigated encryption and chaotic asymmetric memristor-coupled neural networks. This asymmetry makes it more difficult to find hidden attractors because they frequently need highly specific initial conditions for detection and may not exhibit predictable patterns. In unexpected and intricate behaviors, like multi-stability, multiple distinct attractors coexist and produce distinct dynamical outcomes based on the initial conditions and bifurcation parameters. The novel 3D chaotic map with commensurate and incommensurate fractional orders displaying symmetry and asymmetry was examined in [28].

Sigmoidal function provides a new therapeutic approach applicable to many domains [29]. Moreover, robust and highly [30] advanced models can be created by introducing a sigmoidal term and utilizing its intrinsic characteristics; these models have revealed various implementations in encryption and secure communications. Their capacity to seamlessly move from two asymptotic values makes them useful in a variety of fields. For this reason, sigmoidal function systems have drawn the attention of researchers, such as machine learning research [31] and the creation of artificial neural networks [32]. In general, the sigmoidal function generates chaotic models by functioning as a non-linear term. Even their symmetric nature and fixed points are altered with their addition [33]. The intention of this work is to examine and assess the chaotic behavior of a recently suggested incommensurate fractional system. The primary findings and discoveries of this study are outlined as follows:

1. Description of the novel incommensurate fractional discrete memristive system and a basic idea of discrete fractional calculus.
2. The complex non-linear chaotic behavior of a fractional discrete memristive system with incommensurate fractional orders is examined numerically using techniques like the bifurcation, maximum Lyapunov exponent and phase attractors.
3. We use chaos testing including 0-1 test, C_0 complexity and (SampEn) to confirm the complexity in the incommensurate discrete memristive system.
4. Control scheme and chaos synchronization of the presented system are realized according to the stability theorem of discrete non-linear systems.

This paper is detailed as follows: preliminaries of the discrete fractional calculus field and the fractional incommensurate structure of the discrete memristive system are described in Section 2. The existence of hidden chaotic attractors is analyzed numerically, as seen in Section 3. In Section 4, the test of complexity, including the 0-1 test, C_0 complexity and the (SampEn), is employed to verify and quantify chaos in the novel system. The adaptive non-linear controller is a suggested goal that forces the system to converge asymptotically to zero equilibrium and synchronization among the master (drive) and the slave (response) systems analyzed in Section 5. Finally, in Section 6, we discuss the most important results and our plans for future research.

2. Model Description and Preliminaries

This work focuses specifically on the Caputo-like operator to construct a novel incommensurate discrete memristive system.

2.1. Preliminaries

The ϑ -th Caputo-like difference operator ${}^C\Delta_t^\vartheta$ is characterized as [34]

$${}^C\Delta_t^\vartheta Y(\kappa) = \Delta_t^{-(v-\vartheta)} \Delta^v Y(\kappa). \quad (1)$$

$\kappa \in (\mathbb{N})_{t-\vartheta+v}$ and $v = \lceil \vartheta \rceil + 1$, $v - 1 < \vartheta \leq v$. The fractional sum $\Delta_t^{-\vartheta}$ is defined as [35]

$$\Delta_t^{-\vartheta} Y(\kappa) = \frac{1}{\Gamma(\vartheta)} \sum_{a=\vartheta}^{\kappa-\vartheta} (\kappa - a - 1)^{(\vartheta-1)} Y(a), \quad \kappa \in (\mathbb{N})_{v+\vartheta}, \vartheta > 0. \quad (2)$$

where Euler's Gamma function is denoted as

$$\Gamma(\vartheta) = \int_0^\infty t^{\vartheta-1} e^{-t} dt. \quad (3)$$

Next, we introduce the following theorem to derive the fractional discrete system's numerical formula:

Theorem 1 ([36]). *The solution of the following system:*

$$\begin{cases} {}^C\Delta_t^\vartheta Y(\kappa) = h(\kappa - 1 + \vartheta, Y(\kappa + \vartheta - 1)) \\ \Delta^j Y(\kappa) = Y_j, \quad v = \lceil \vartheta \rceil + 1, \end{cases} \quad (4)$$

is given by

$$Y(\kappa) = Y_0(t) + \frac{1}{\Gamma(\vartheta)} \sum_{a=v-\vartheta}^{\kappa-\vartheta} (\kappa - a)^{(\vartheta-1)} g(a + \vartheta - 1, Y(a + \vartheta - 1)), \quad \kappa \in \mathbb{N}_{t+v}, \quad (5)$$

where

$$Y_0(t) = \sum_{j=0}^{v-1} \frac{(k-t)^j}{\Gamma(n+1)} \Delta^j Y(t). \quad (6)$$

Take $t = 0$, $j = \vartheta - 1 + a$, for $\vartheta \in (0, 1]$ and $v = 1$, $(\kappa - a - 1)^{(\vartheta-1)} = \frac{\Gamma(\kappa-\ell)}{\Gamma(\kappa-\ell-\vartheta+1)}$, the numerical Formula (5) is written as

$$Y(\kappa) = Y(0) + \frac{1}{\Gamma(\vartheta)} \sum_{j=0}^{\kappa-1} \frac{\Gamma(\kappa - n + \vartheta - 1)}{\Gamma(\kappa - n)} h(j, Y(j)). \quad (7)$$

Now, the theorem below is practiced to value the stability under incommensurate orders of discrete fractional non-linear models.

Theorem 2 ([37]). *Consider the system*

$$\begin{cases} {}^C\Delta_t^{\vartheta_1}y_1(\kappa) = Y_1(y(\kappa - 1 + \vartheta_1)), \\ {}^C\Delta_t^{\vartheta_2}y_2(\kappa) = Y_2(y(\kappa - 1 + \vartheta_2)), \\ \vdots \\ {}^C\Delta_t^{\vartheta_n}y_n(\kappa) = Y_n(y(\kappa - 1 + \vartheta_n)). \end{cases} \quad \kappa = 0, 1, \dots, \tag{8}$$

Let $y(\kappa) = (y_1(\kappa), \dots, y_n(\kappa))^T \in \mathbb{R}^n$, $Y = (Y_1, \dots, Y_n) : \mathbb{R}^n \rightarrow \mathbb{R}^n$, Let $\vartheta_i \in (0, 1]$, $i = \overline{1, n}$, and M is the (LCM) of the denominators \bar{v}_i of ϑ_i added to $\vartheta_i = \frac{\bar{v}_i}{v_i}$, $(\bar{v}_i, v_i) = 1$, $\bar{v}_i, v_i \in \mathbb{Z}_+, \forall i = \overline{1, n}$.

$$\det(\text{diag}(\lambda^{M\vartheta_1}, \dots, \lambda^{M\vartheta_n}) - (1 - \lambda^M)B) = 0, \tag{9}$$

if each root of (9) involved in \mathbb{C}/K^q as B represents the Jacobian matrix of (8) and $q = \frac{1}{M}$

$$K^q = \left\{ \eta \in \mathbb{C} : |\eta| \leq \left(2 \cos \frac{|\text{arg}\eta|}{q} \right)^q \text{ and } |\text{arg}\eta| \leq \frac{q\pi}{2} \right\}. \tag{10}$$

It follows that (8) has an asymptotically stable zero solution.

2.2. Description of the Incommensurate System

In [38], Bao et al. found that the suggested memristive map displayed multistable behavior. On the other hand, the sigmoidal functions are renowned for their unique non-linear characteristics and ability to change data. Very recently, innovative dynamical systems with particular characteristics could be produced by incorporating this function and the memristive map into the design of discrete chaotic systems. In this work, based on [39,40], we produce the novel incommensurate discrete memristive system using the difference operator ${}^C\Delta_t^{\vartheta_i}$, which can be represented as follows:

$$\begin{aligned} {}^C\Delta_t^{\vartheta_1}y_1(\kappa) &= \frac{\alpha_1}{1 + e^{-\beta y_1(\kappa + \vartheta_1 - 1)}} + \alpha_2 y_1(\kappa + \vartheta_1 - 1)((y_2(\kappa + \vartheta_1 - 1))^2 - 1) - y_1(\kappa + \vartheta_1 - 1), \\ {}^C\Delta_t^{\vartheta_2}y_2(\kappa) &= y_1(\kappa + \vartheta_2 - 1), \end{aligned} \tag{11}$$

where α_1, β and α_2 are the influence of the system.

2.3. Equilibrium Points Analysis

Through solving the following equation system, the (y_1^*, y_2^*) equilibrium points of the incommensurate discrete memristive system (11) can be found:

$$\begin{cases} \frac{\alpha_1}{1 + e^{-\beta y_1^*}} + \alpha_2 y_1^*((y_2^*)^2 - 1) - y_1^* = 0, \\ y_1^* = 0. \end{cases} \tag{12}$$

From Equation (2) of (12), $y_1^* = 0$, replacing y_1^* in Equation (1), for $\alpha_1 \neq 0$ it becomes apparent that the system (12) has no solution. Therefore, the incommensurate discrete memristive system (11) can create hidden chaotic attractors and exhibits asymmetry if $\alpha_1 \neq 0$ as shown in Figure 1. For more details, hidden attractors may manifest in a symmetric dynamic manner that preserves the symmetry of the system; their trajectories may mirror or repeat within symmetrical boundaries of the phase space of the incommensurate discrete memristive system. This may result in periodic or symmetric chaotic behavior,

whereas hidden attractors may show skewed or irregular dynamics in asymmetric dynamic, disrupting the system’s apparent regularity. Our results indicate that the hidden attractor does not originate from the local dynamics around the equilibrium points. This confirms that the attractor is hidden, as it can only be detected under specific initial conditions away from the vicinity of equilibrium.

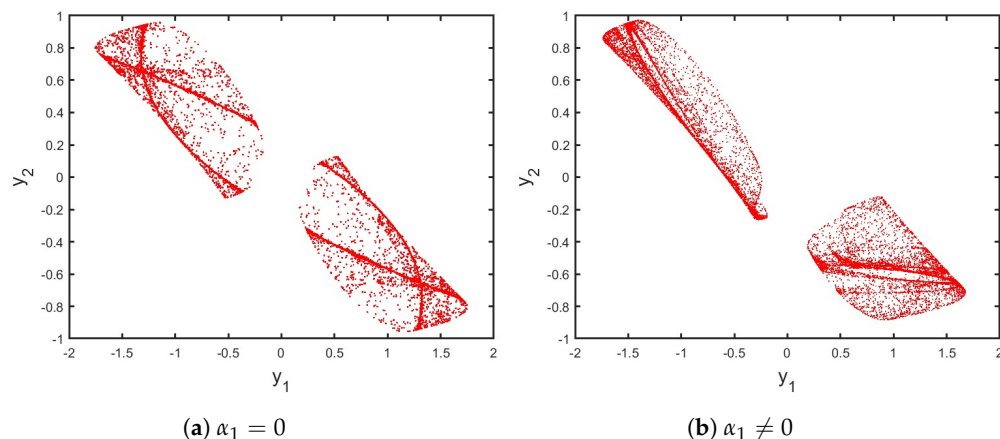


Figure 1. (a) Symmetry for $\alpha_1 = 0, \beta = 0.5$ and $\alpha_2 = 1.75$, (b) asymmetry for $\alpha_1 = 0.16, \beta = 0.5$ and $\alpha_2 = 1.75$.

3. Existence of Hidden Chaotic Attractors

The main subject of this section is studying the dynamics of the novel incommensurate discrete memristive system. The following describes the numerical formula of (11) based on Theorem 1:

$$\begin{cases} y_1(\kappa) = y_1(0) + \frac{1}{\Gamma(\theta_1)} \sum_{j=0}^{\kappa} \frac{\Gamma(\kappa-1-j+\theta_1)}{\Gamma(\kappa-j)} \left(\frac{\alpha_1}{1+e^{-\beta y_1(j)}} + \alpha_2 y_1(j) ((y_2(j))^2 - 1) - y_1(j) \right), \\ y_2(\kappa) = y_2(0) + \frac{1}{\Gamma(\theta_2)} \sum_{j=0}^{\kappa} \frac{\Gamma(\kappa-1-j+\theta_2)}{\Gamma(\kappa-j)} (y_1(j)). \quad \kappa = 1, 2, \dots \end{cases} \tag{13}$$

In order to understand a chaos theory in the fractional system, we use the Jacobian matrix technique [41] to find the maximum Lyapunov exponents (LE_{max}), where J_a is characterized by

$$J_a = \begin{pmatrix} F_1(a) & F_2(a) \\ W_1(a) & W_2(a) \end{pmatrix}, \tag{14}$$

where

$$\begin{cases} F_1(a) = F_1(0) + \frac{1}{\Gamma(\theta_1)} \sum_{j=0}^{a-1} \frac{\Gamma(\theta_1+a-j-1)}{\Gamma(a-j)} \left(\frac{\beta \alpha_1 e^{-\beta y_1(j)}}{(1+e^{-\beta y_1(j)})^2} + \alpha_2 (y_2(j)^2 - 1) - 1 \right) F_1(j) + \\ \quad (2y_2(j)\alpha_2 y_1(j))W_1(j), \\ F_2(a) = F_2(0) + \frac{1}{\Gamma(\theta_1)} \sum_{j=0}^{a-1} \frac{\Gamma(\theta_1+a-j-1)}{\Gamma(a-j)} \left(\frac{\beta \alpha_1 e^{-\beta y_1(j)}}{(1+e^{-\beta y_1(j)})^2} + \alpha_2 (y_2(j)^2 - 1) - 1 \right) F_2(j) + \\ \quad (2y_2(j)\alpha_2 y_1(j))W_2(j), \\ W_1(a) = W_1(0) + \frac{1}{\Gamma(\theta_2)} \sum_{j=0}^{a-1} \frac{\Gamma(\theta_2+a-j-1)}{\Gamma(a-j)} F_1(j), \\ W_2(a) = W_2(0) + \frac{1}{\Gamma(\theta_2)} \sum_{j=0}^{a-1} \frac{\Gamma(\theta_2+a-j-1)}{\Gamma(a-j)} F_2(j). \end{cases} \tag{15}$$

where

$$\begin{pmatrix} F_1(0) & F_2(0) \\ W_1(0) & W_2(0) \end{pmatrix} = \begin{pmatrix} 1 & 0 \\ 0 & 1 \end{pmatrix}. \tag{16}$$

Then, the LE_t of the fractional system can be given by

$$LE_t = \lim_{a \rightarrow \infty} \frac{1}{a} \ln |\lambda_t^{(a)}|, \quad \text{for } t = 1, 2, \tag{17}$$

where $\lambda_t^{(a)}$ are the eigenvalues of J_a .

Set the parameters $\alpha_1 = 0.16$, $\alpha_2 = 1.75$, $\beta = 0.5$ and the initial condition (IN): $(y_1(0), y_2(0)) = (-0.3, 0.3)$. First, Figure 2 portrays the evolution states of the incommensurate discrete memristive system (11) for $(\vartheta_1, \vartheta_2) = (1, 0.97)$, while the resulting hidden asymmetry chaotic attractor for different incommensurate orders $(\vartheta_1, \vartheta_2)$ as shown in Figure 3. Therefore, these findings show that the form of the hidden attractors of (11) is affected by the selection of the incommensurate orders.

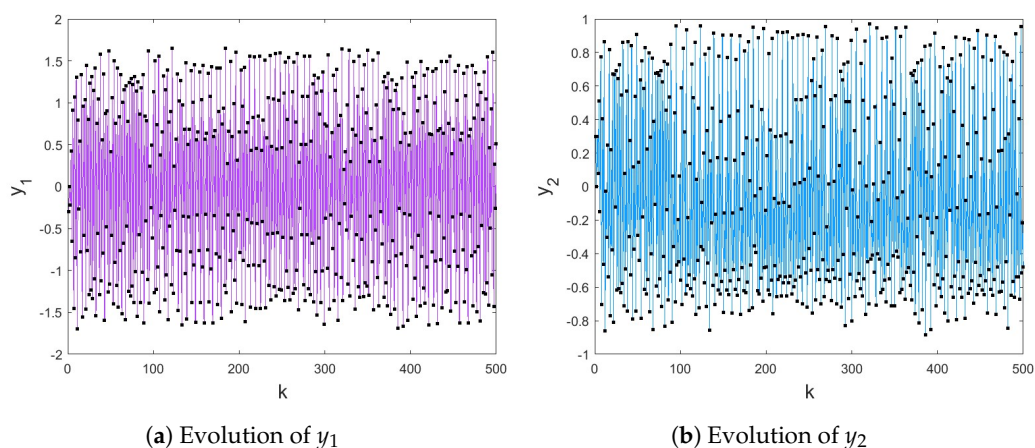


Figure 2. Time evolution of (11) for $(\vartheta_1, \vartheta_2) = (1, 0.97)$ with IN.

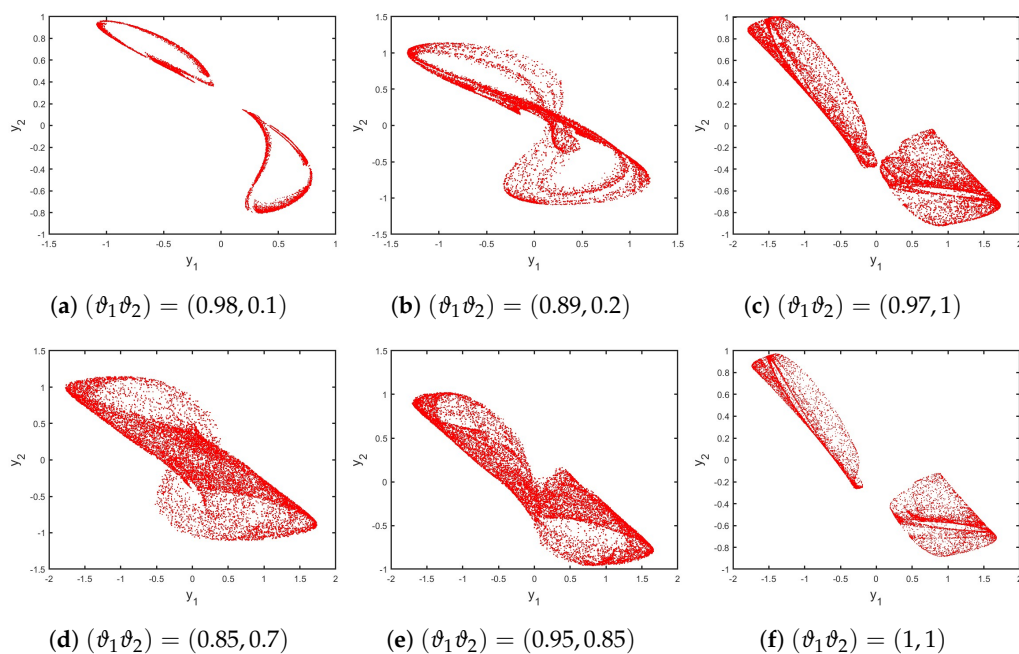


Figure 3. Hidden attractors of (11) for various incommensurate order $(\vartheta_1, \vartheta_2)$ and IN.

Case 1: In this case, to gain a deeper comprehension of the influence of incommensurate orders on the evolution of (11), we change ϑ_1 and ϑ_2 , the incommensurate orders, so that the stability region shrinks and the chaotic area expands. From Figure 4, we provide bifurcation charts along with the related plots LE_{max} when versus $\vartheta_1 \in [0.75, 1]$ and we choose $\vartheta_2 = 1$, we can see that the states become totally

chaotic where the LE_{max} values are positive. As seen in Figure 5, versus $\vartheta_2 \in (0, 1]$ and we fixed the incommensurate order as $\vartheta_1 = 1$ so that the trajectories of the proposed incommensurate discrete memristive system (11) move adaptability between a stable motion and a hidden chaotic. When $\vartheta_2 \in [0, 0.19]$, it is observed that the discrete system exhibits stable trajectories with the periodic motion 2, 6 and 12-period orbits, while it is periodic in $[0.45, 0.55]$. When $\vartheta_2 \in [0.2, 0.44] \cup [0.56, 0.6]$ the LE_{max} gradually increase which indicates the existence of chaos. In addition, when ϑ_2 increases until it approaches 1 where the LE_{max} until their highest values, the incommensurate discrete memristive system (11) becomes totally chaotic. Consequently, numerous values of the incommensurate derivative affect the rich dynamics of (11).

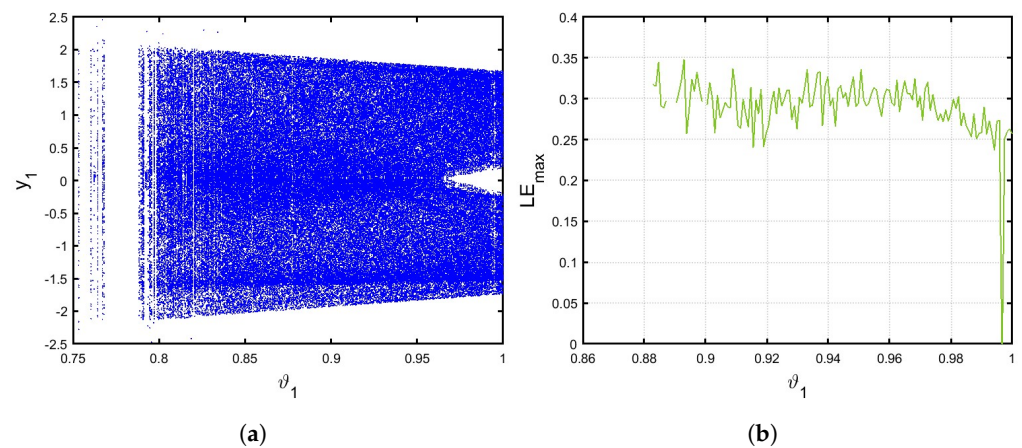


Figure 4. (a) Bifurcation of (11) for $\vartheta_1 \in [0.7, 1]$, $\vartheta_2 = 1$. (b) The associated LE_{max} .

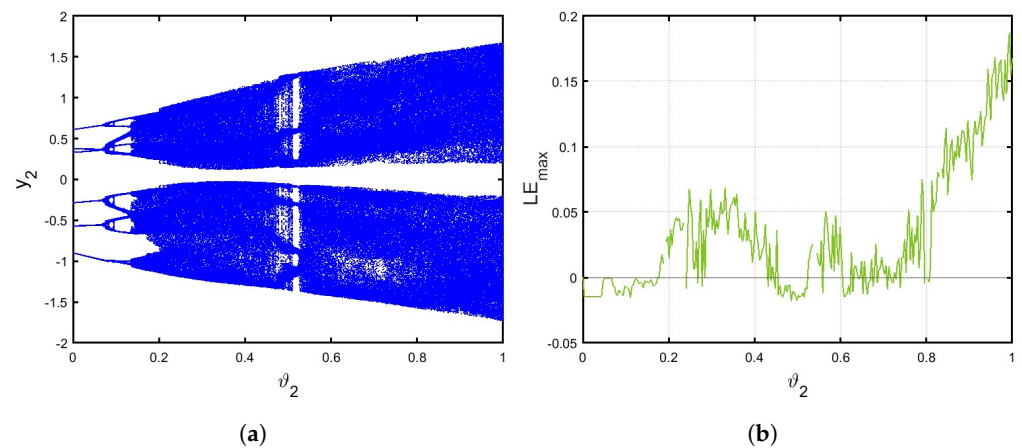


Figure 5. (a) Bifurcation of (11) for $\vartheta_2 \in (0, 1]$, $\vartheta_1 = 1$. (b) The associated LE_{max} .

Case 2: Figure 6 displays two bifurcation diagrams and their associated graph of LE_{max} for α_1 versus in $[0, 0.3]$ correspond to the incommensurate values $(\vartheta_1, \vartheta_2) = (0.9, 0.1)$ and $(\vartheta_1, \vartheta_2) = (1, 0.97)$. We can see that, when $(\vartheta_1, \vartheta_2) = (0.9, 0.1)$, the trajectories of the a novel incommensurate discrete memristive system (11) are totally chaotic in the interval $[0, 0.3]$. When $(\vartheta_1, \vartheta_2) = (1, 0.97)$, the dynamics of the system shift from periodic to chaotic. If $\alpha_1 < 0.003$, there is periodic behavior where LE_{max} values are negative; otherwise, if α_1 increases the LE_{max} takes their higher values, indicating that the chaotic region expanded.

Now, in Figure 7 versus α_2 in $[1.5, 1.9]$ and when choosing $\alpha_1 = 0.16$, the trajectories exhibit the system ranging from periodic to chaotic. Specifically, Figure 7a shows that the behaviors of the incommensurate discrete memristive system (11) transition between regular and period-doubling bifurcation. When α_2 at $[1.5, 1.625]$, the trajectories are periodic with negative values of LE_{max} , while when $1.625 < \alpha_2 < 1.88$, the system becomes period-doubling bifurcation where the LE_{max} values are positive, as shown in Figure 7b. Furthermore, when α_2 increases, the system exhibits a divergence towards infinity. In addition, in Figure 7c, we can see that the chaotic motions appear when $\alpha_2 \in [1.68, 1.718] \cup [1.722, 1.88]$, while $\alpha_2 \in [1.5, 1.679]$ show periodic windows with 2-period orbits, at $[1.719, 1.721]$ also indicating the periodic orbit of the system where the LE_{max} alternates between positive values and negative values, as seen in Figure 7d. When α_2 increases and becomes close to 1.9, the map the chaotic region expanded. It is apparent that the behaviors of (11) are influenced by the incommensurate derivative order $(\vartheta_1, \vartheta_2) = (1, 1)$. It is simple to see that the two suggested incommensurate derivatives have distinct shapes.

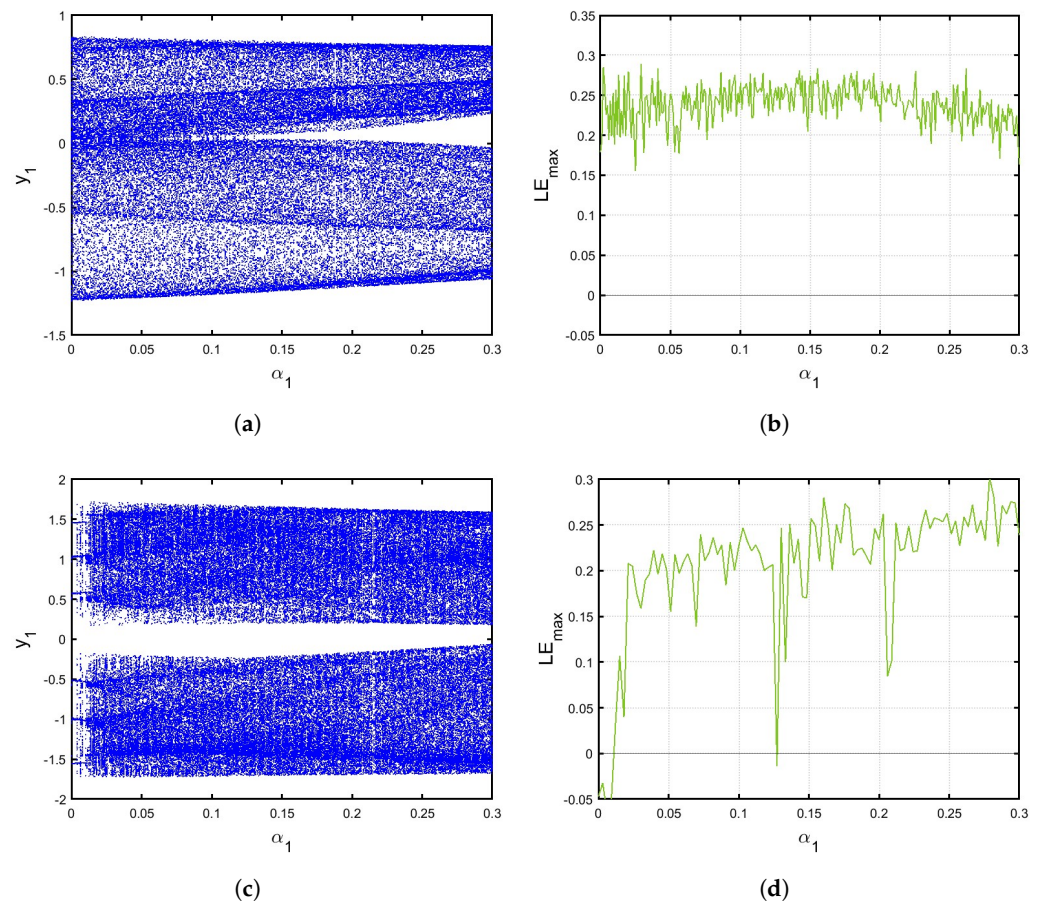


Figure 6. Bifurcation and the associated LE_{max} of (11) versus α_1 for (a,b) $(\vartheta_1, \vartheta_2) = (0.9, 0.1)$; (c,d) $(\gamma_1, \gamma_2) = (1, 0.97)$.

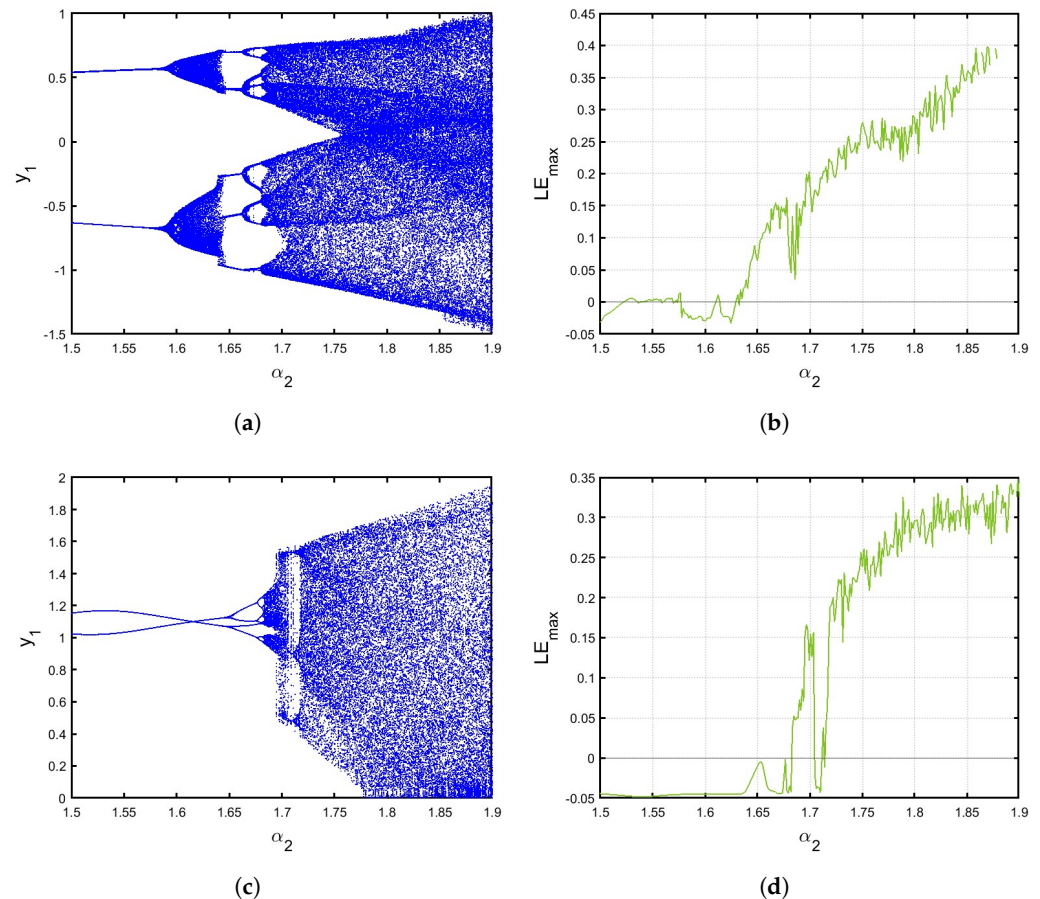


Figure 7. Bifurcation and the associated LE_{max} of (11) versus α_2 for (a,b) $(\theta_1, \theta_2) = (0.9, 0.1)$; (c,d) $(\theta_1, \theta_2) = (1, 0.97)$.

4. Chaotic Test and Entropy

In this section, we focus on examining the incommensurate discrete memristive system's chaotic motion and complexity. We use the C_0 Complexity algorithm, the sample entropy approach (SampEn) and the 0-1 test to verify and assess the degree of chaos in the system. Using these techniques, we discover that the chaotic region of the discrete system is amplified in proportion to the complexity measures. This relationship emphasizes the connection between chaos and complexity, showing how the discrete memristive system's behavior is greatly enhanced by introducing incommensurate orders, leading to more complex and prominent chaotic phenomena.

4.1. 0-1 Test

The 0-1 test [42] is particularly advantageous for the affirmation of areas of chaos and uniform behavior of the novel incommensurate discrete system (11). Initially, we present the translation component as follows:

$$p_b(s) = \sum_{\zeta=1}^s x(\zeta) \cos(\zeta b), \quad q_b(s) = \sum_{\zeta=1}^s x(\zeta) \sin(\zeta b), \quad (18)$$

where the translation variables are represented by $x(\zeta), \zeta = \overline{1, N}$, and the constant $b \in in(0, \pi)$ is chosen at random. Next, the meaning of mean square displacement is as follows:

$$M_b(s) = \lim_{N \rightarrow \infty} \frac{1}{N} \sum_{\zeta=1}^N \left[(p_b(\zeta + s) - p_b(\zeta))^2 + (q_b(\zeta + s) - q_b(\zeta))^2 \right], \quad \zeta \leq \frac{N}{10}. \quad (19)$$

Additionally, K_b , the rate of asymptotic growth, is represented by

$$K_b = \lim_{s \rightarrow \infty} \frac{\log M_b(s)}{\log \zeta}. \quad (20)$$

Plotting p_b, q_b is employed to determine whether or not chaos exists. So, if $K = \text{median}(K_b)$ is close to 1, the dynamics of (11) will be chaotic; otherwise, it will become regular as K approaches 0 and p_b, q_b exhibits bounded-like behavior.

Therefore, the $p - q$ plots of the incommensurate discrete memristive system (11) for different incommensurate values can be seen in Figure 8. Particularly, when $(\vartheta_1, \vartheta_2) = (1, 0.01)$ in Figure 8a and $(\vartheta_1, \vartheta_2) = (1, 0.48)$ in Figure 8b they display bounded-like states, indicating a periodic nature of the system. When $(\vartheta_1, \vartheta_2) = (0.9, 0.1)$, they show Brownian-like states. Figure 8c and $(\vartheta_1, \vartheta_2) = (1, 0.97)$, as well as Figure 8d affirm that the incommensurate system is chaotic. Then, these findings are consistent with the bifurcation and (*LEmax*).

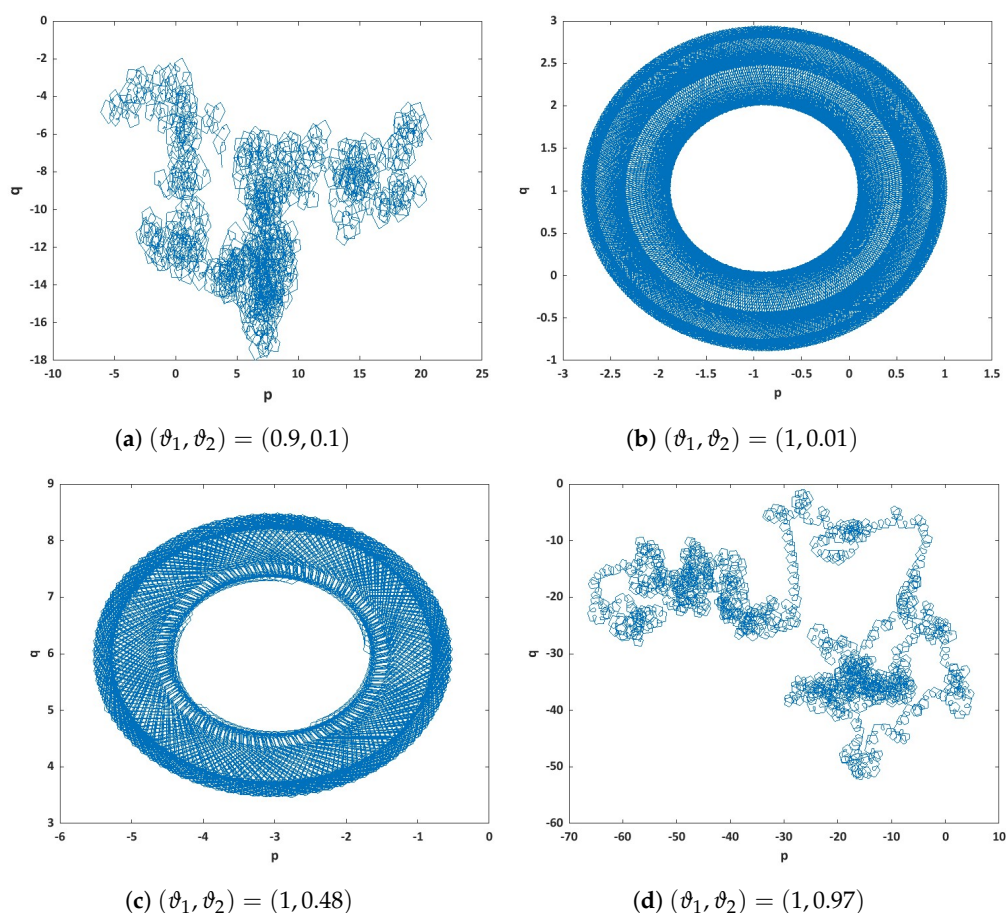


Figure 8. The 0-1 test of the incommensurate discrete memristive system (11).

4.2. The Sample Entropy

The complexity of the incommensurate discrete memristive system (11) is measured using the sample entropy (SampEn) [43,44] in this part when large values of SampEn signify a greater level of complexity. The SampEn algorithm is considered as follows:

$$\text{SampEn} = -\log \frac{\Theta^{j+1}(\mu)}{\Theta^j(\mu)}, \quad (21)$$

where $\Theta^j(\mu)$ is given by

$$\Theta^j(\mu) = \frac{1}{\bar{l} - j + 1} \sum_{j=1}^{\bar{l} - j + 1} \log C_j^i(\mu), \tag{22}$$

with $\mu = 0.2std(x)$.

Figure 9 displays the approximate sample entropy of the incommensurate discrete memristive system (11), with $\beta = 0.5$, IN. However, the larger sample entropy values of the incommensurate system (11) demonstrate the higher complexity of the system, as indicated by the results of (SampEn), which is in agreement with the *LEmax* analysis.

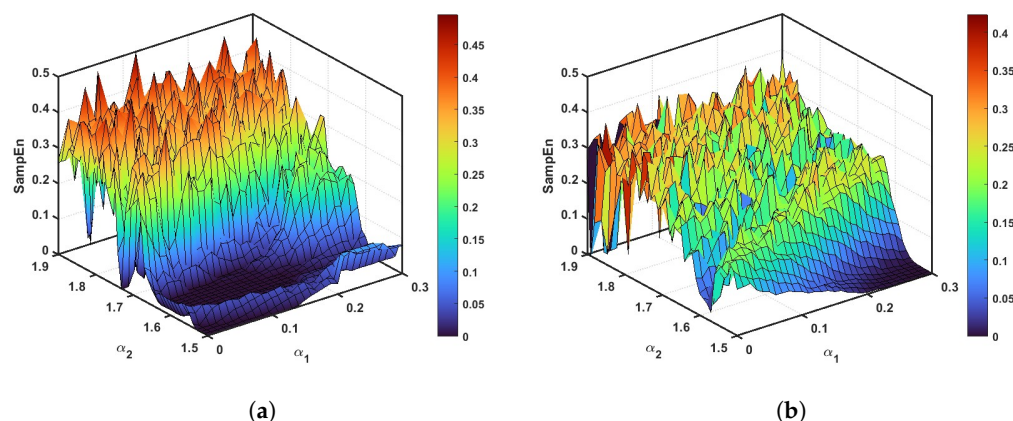


Figure 9. SampEn of (11) versus α_1 and α_2 for (a) $(\vartheta_1, \vartheta_2) = (1, 0.97)$, (b) $(\vartheta_1, \vartheta_2) = (0.9, 0.1)$.

4.3. C_0 Complexity

In this part, employing the C_0 complexity method [45], which is derived from the inverse Fourier transform, we measured the complexity of the incommensurate discrete memristive system (11).

The methodology for $\{\Omega(\sigma), \sigma = 1, \dots, Q - 1\}$ is explained from the following:

- The Fourier transform of $\Omega(\sigma)$ is ascertained by

$$\chi_Q(\sigma) = \frac{1}{Q} \sum_{\sigma=0}^{Q-1} \Omega(\sigma) \exp^{-2\pi i(\frac{kj}{Q})}, \quad \sigma = 0, 1, \dots, Q - 1. \tag{23}$$

- Explaining the mean square of $\chi_Q(\sigma)$ as $G_Q = \frac{1}{Q} \sum_{\sigma=0}^{Q-1} |\chi_Q(\sigma)|^2$, set

$$\bar{\chi}_Q(\sigma) = \begin{cases} \chi_Q(\sigma) & \text{if } \|\chi_Q(\sigma)\|^2 > rG_Q, \\ 0 & \text{if } \|\chi_Q(\sigma)\|^2 \leq rG_Q. \end{cases} \tag{24}$$

- To find the inverse Fourier transform, use the following expression:

$$\rho(j) = \frac{1}{Q} \sum_{\sigma=0}^{Q-1} \bar{\chi}_Q(\sigma) \exp^{2\pi i(\frac{j\sigma}{Q})}, \quad j = 0, 1, \dots, Q - 1. \tag{25}$$

- The C_0 complexity is determined by using the ensuing formula:

$$C_0 = \frac{\sum_{j=0}^{Q-1} \|\rho(j) - \Omega(j)\|}{\sum_{j=0}^{Q-1} \|\Omega(j)\|^2}. \tag{26}$$

Figure 10 shows the C_0 complexity of the incommensurate discrete memristive system (11). Specifically, Figure 10a versus $\vartheta_1 \in [0.75, 1]$ for $\vartheta_2 = 1$ while Figure 10b versus $\vartheta_2 \in (0, 1]$ for $\vartheta_1 = 1$ where $\alpha_1 \in [0, 0.3]$ are versus parameter for $\alpha_2 = 1.75$. Meanwhile, Figure 10c $\alpha_2 \in [1.5, 1.9]$ are versus parameter for $\alpha_1 = 0.16$ where $\vartheta_1 \in [0.75, 1]$ versus for $\vartheta_2 = 1$ and Figure 10d versus $\vartheta_2 \in (0, 1]$ for $\vartheta_1 = 1$. The systems' higher complexity is confirmed by the C_0 complexity results. These outcomes are consistent with the previously mentioned findings.

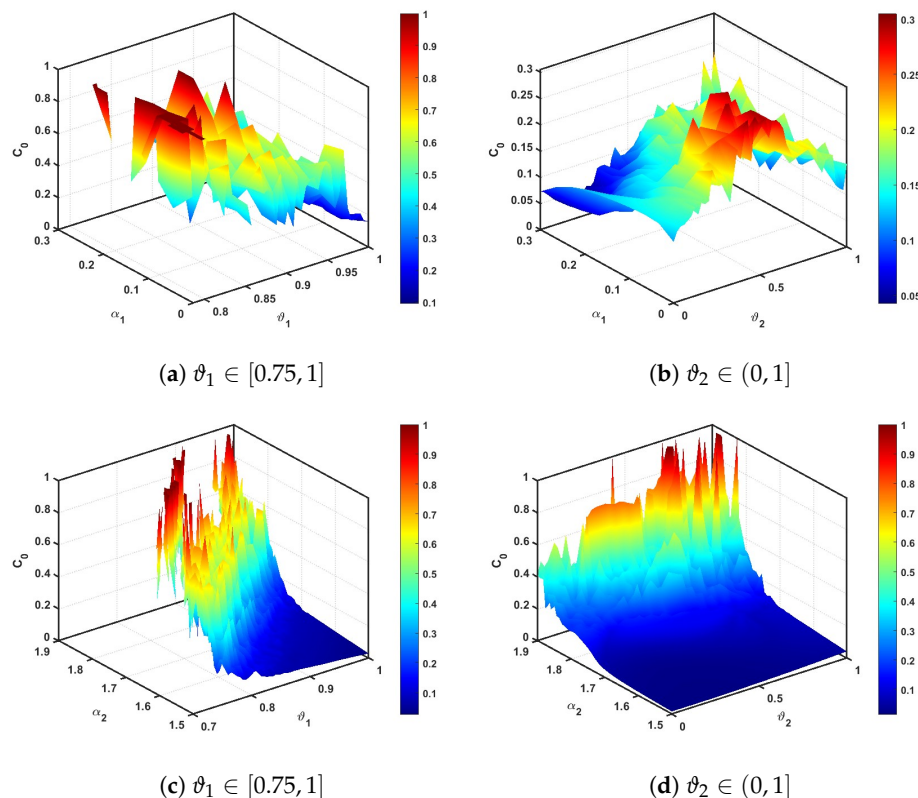


Figure 10. The C_0 complexity of (11) versus ϑ_1, ϑ_2 and (a,b) $\alpha_1 \in [0, 0.3]$, (c,d) $\alpha_2 \in [1.5, 1.9]$.

5. Chaos Control Approaches

The stability analysis and synchronization schema of the incommensurate discrete memristive system (11) are covered in this section. Presenting the following propositions, which serve as the foundation for examining the stabilization and synchronization of incommensurate discrete systems, is our first goal. The efficacy of the suggested control strategy is then shown through numerical simulations.

5.1. Stabilization

In this part, we stabilize the suggested incommensurate discrete memristive system (11) by guaranteeing the stability conditions that each state of the system converges to zero.

The following describes the controlled system of the incommensurate discrete system:

$$\begin{cases} {}^C\Delta_t^{\vartheta_1} y_1(\kappa) = \frac{\alpha_1}{1 + e^{-\beta y_1(\kappa + \vartheta_1 - 1)}} + \alpha_2 y_1(\kappa + \vartheta_1 - 1) ((y_2(\kappa + \vartheta_1 - 1))^2 - 1) - \\ \quad y_1(\kappa + \vartheta_1 - 1) + \mathbf{L}_1(\kappa + \vartheta_1 - 1), \\ {}^C\Delta_t^{\vartheta_2} y_2(\kappa) = y_1(\kappa + \vartheta_2 - 1) + \mathbf{L}_2(\kappa + \vartheta_2 - 1), \end{cases} \tag{27}$$

where $\mathbf{L} = (\mathbf{L}_1, \mathbf{L}_2)^T$ is the adaptive controller. Next, the stabilization of the system is governed by the following control:

Proposition 1. *The incommensurate system (11) is stable employing the 2D control*

$$\begin{cases} L_1(\kappa + \vartheta_1 - 1) = -\frac{\alpha_1}{1 + e^{-\beta y_1(\kappa + \vartheta_1 - 1)}} - \alpha_2 y_1(\kappa + \vartheta_1 - 1)(y_2(\kappa + \vartheta_1 - 1))^2 + \\ \alpha_2 y_1(\kappa + \vartheta_1 - 1), \\ L_2(\kappa + \vartheta_2 - 1) = -\frac{1}{2}y_2(\kappa + \vartheta_2 - 1). \end{cases} \tag{28}$$

Proof Substituting (28) by (27), we obtain the subsequent system outcomes:

$$\begin{cases} {}^C\Delta_t^{\vartheta_1}y_1(\kappa) = -y_1(\kappa + \vartheta_1 - 1), \\ {}^C\Delta_t^{\vartheta_2}y_2(\kappa) = y_1(\kappa + \vartheta_2 - 1) - \frac{1}{2}y_2(\kappa + \vartheta_2 - 1). \end{cases} \tag{29}$$

So

$$\det(\text{diag}(\lambda^{M\vartheta_1}, \lambda^{M\vartheta_2} - (1 - \lambda^M)B) = 0,$$

where $M = 100$,

$$B = \begin{pmatrix} -1 & 0 \\ 1 & -\frac{1}{2} \end{pmatrix}. \tag{30}$$

For $(\vartheta_1, \vartheta_2) = (1, 0.97)$

$$\det\left(\begin{pmatrix} \lambda^{100} & 0 \\ 1 & \lambda^{97} \end{pmatrix} - (1 - \lambda^{100})K\right) = 0,$$

\Leftrightarrow

$$\lambda^{197} - 0.5\lambda^{110} - \lambda^{107} + 0.5\lambda^{100} + \lambda^{97} + 0.5\lambda^{20} - \lambda^{10} + 0.5 = 0. \tag{31}$$

Based on Theorem 2, and since a consequence of $\lambda_j \in \mathbb{C}/K^{\frac{1}{100}}$, ($j = \overline{1, 197}$), in the direction of $(0, 0)$, the (27) is asymptotically stable. Figure 11 highlights the stabilization of the controlled incommensurate discrete memristive system (27) for $(\vartheta_1, \vartheta_2) = (1, 0.97)$ by showing how the system asymptotically becomes $(0, 0)$.

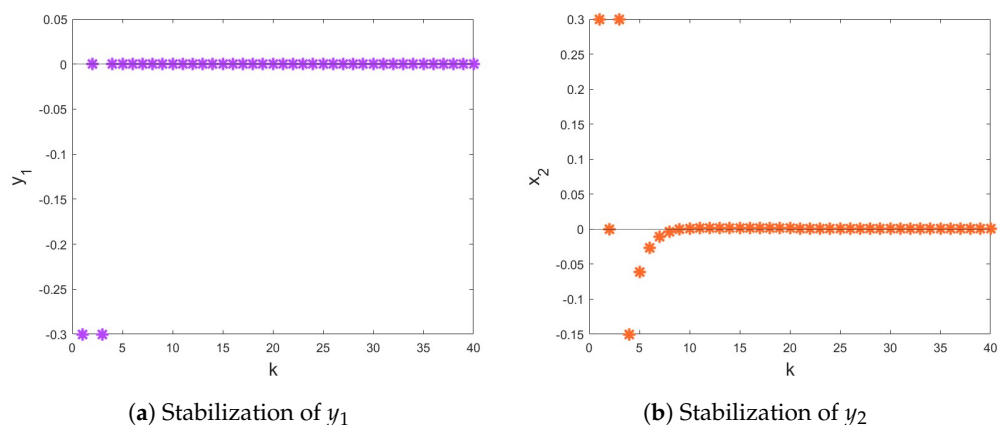
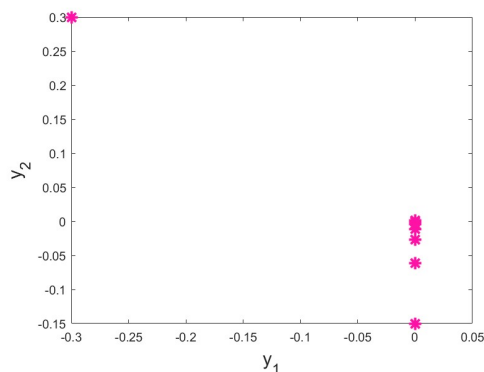


Figure 11. *Cont.*



(c) Attractor

Figure 11. The stabilized states and attractors of the controlled (27) for $(\vartheta_1, \vartheta_2) = (1, 0.97)$.

5.2. Synchronization

In order to synchronize the states of the drive and the response chaotic models, control parameters are added to the response system. This forces the response system states towards those of the drive chaotic discrete system. Therefore, the incommensurate discrete memristive system (11) is regarded as the "Drive" system and defines the "Response" in the following manner:

$$\begin{cases} {}^C\Delta_t^{\vartheta_1} y_{1m}(\kappa) = \frac{\alpha_1}{1 + e^{-\beta y_{1m}(\kappa + \vartheta_1 - 1)}} + \alpha_2 y_{1m}(\kappa + \vartheta_1 - 1) ((y_{2m}(\kappa + \vartheta_1 - 1))^2 - 1) - \\ \quad y_{1m}(\kappa + \vartheta_1 - 1) + \mathbf{N}_1(\kappa + \vartheta_1 - 1), \\ {}^C\Delta_t^{\vartheta_2} y_{2m}(\kappa) = y_{1m}(\kappa + \vartheta_2 - 1) + \mathbf{N}_2(\kappa + \vartheta_2 - 1). \end{cases} \quad (32)$$

$\mathbf{N}_1, \mathbf{N}_2$ signify the synchronization controllers. The following yields the fractional error map:

$$\begin{cases} {}^C\Delta_t^{\vartheta_1} e_1(\kappa) = \alpha_1 \left(\frac{1}{1 + e^{-\beta y_{1m}(\kappa + \vartheta_1 - 1)}} - \frac{1}{1 + e^{-\beta y_1(\kappa + \vartheta_1 - 1)}} \right) - \alpha_2 e_1(\kappa + \vartheta_1 - 1) ((y_2(\kappa + \vartheta_1 - 1))^2 \\ \quad - y_{2m}(\kappa + \vartheta_1 - 1))^2) + \alpha_2 e_1(\kappa + \vartheta_1 - 1) + e_1(\kappa + \vartheta_1 - 1) + \mathbf{N}_1(\kappa + \vartheta_1 - 1), \\ {}^C\Delta_t^{\vartheta_2} e_2(\kappa) = e_1(\kappa + \vartheta_2 - 1) + \mathbf{N}_2(\kappa + \vartheta_2 - 1). \end{cases} \quad (33)$$

where the synchronization error is characterized as

$$\begin{cases} e_1(\kappa) = y_{1m}(\kappa) - y_1(\kappa), \\ e_2(\kappa) = y_{2m}(\kappa) - y_2(\kappa), \end{cases} \quad (34)$$

$$\lim_{\kappa \rightarrow \infty} \| e_j(\kappa) \| = 0, \forall j = 1, 2.$$

Proposition 2. Subject to

$$\begin{cases} \mathbf{N}_1(\kappa + \vartheta - 1) = -\alpha_2 e_1(\kappa + \vartheta_1 - 1) - \alpha_1 \left(\frac{1}{1 + e^{-\beta y_{1m}(\kappa + \vartheta_1 - 1)}} - \frac{1}{1 + e^{-\beta y_1(\kappa + \vartheta_1 - 1)}} \right) + \\ \quad \alpha_2 e_1(\kappa + \vartheta_1 - 1) ((y_2(\kappa + \vartheta_1 - 1))^2 - y_{2m}(\kappa + \vartheta_1 - 1))^2), \\ \mathbf{N}_2(\kappa + \vartheta_2 - 1) = -\frac{1}{2} e_2(\kappa + \vartheta_2 - 1). \end{cases} \quad (35)$$

Then, there is a synchronization between the response system (32) and the drive (11).

Proof. Substituting (35) into the error system (36), we obtain

$$\begin{cases} {}^C\Delta_t^{\vartheta_1} e_1(\kappa) = -e_1(\kappa + \vartheta_1 - 1), \\ {}^C\Delta_t^{\vartheta_2} e_2(\kappa) = e_1(\kappa + \vartheta_2 - 1) - \frac{1}{2}e_2(\kappa + \vartheta_2 - 1), \end{cases} \quad (36)$$

\Leftrightarrow

$${}^C\Delta_t^{\vartheta_i}(e_1(\kappa), e_2(\kappa))^T = B(e_1(\kappa + \vartheta_i - 1), e_2(\kappa + \vartheta_i - 1))^T, \quad i = 1, 2. \quad (37)$$

where

$$B = \begin{pmatrix} -1 & 0 \\ 1 & -\frac{1}{2} \end{pmatrix}. \quad (38)$$

Thus, the eigenvalues of B are $\lambda_1 = -1$, $\lambda_2 = -\frac{1}{2}$, which satisfy the condition of Theorem 2. Then, the control law (35) realizes the synchronization of the drive (11) and the response (32) incommensurate discrete memristive system. Using numerical simulations, this outcome is shown, wherein we chose $(e_1(0), e_2(0)) = (-0.1, -0.1)$, and Figure 12 displays the states and attractor of the error (36). Evidently, the errors are getting closer to zero, which confirms the synchronization outcomes. \square

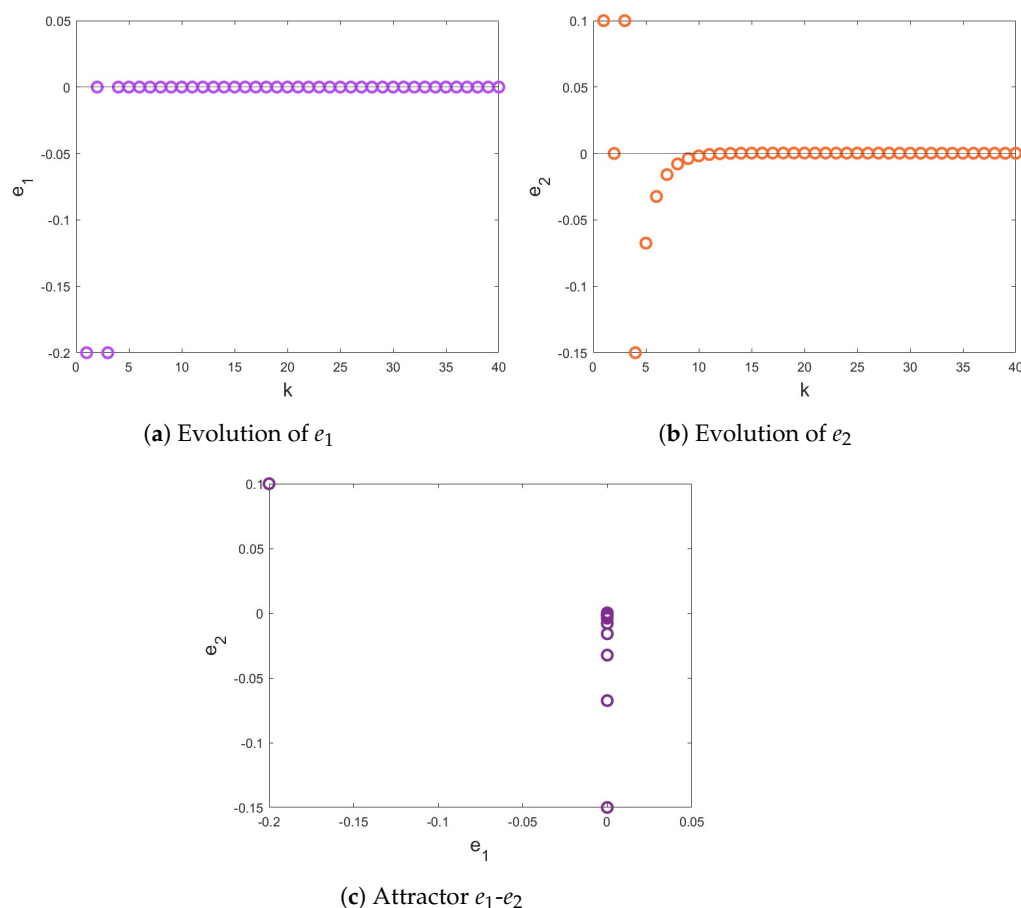


Figure 12. Synchronization of the error system (36).

6. Conclusions and Perspectives

This paper introduces a novel fractional discrete memristive system with incommensurate orders. It thoroughly studies the influence of incommensurate fractional orders on the system’s dynamics and behavior.

First, asymmetric analysis of the system without a fixed point that also varied the parameters or derivative fractional values showed that the system can exhibit a variety

of intricate hidden dynamical behaviors. Second, the quantitative evaluation of system complexity was confirmed by the 0-1 test, the (SampEn) method and C_0 Complexity. Third, efficient control laws that can ensure the stabilization and synchronization of the incommensurate discrete memristive system states while forcing them to approach asymptotic zero were developed. Lastly, the outcomes were shown through numerical simulations conducted using MATLAB R2024a.

Future work should take into account memristive maps based on certain phenomena, as they are valuable in understanding the implications of fractional chaotic memristive map and furthering the study of chaotic dynamics systems.

Author Contributions: Conceptualization, M.A.H. and M.A.; Data curation, H.A.-T. and A.O.; Formal analysis, M.A. and L.D.; Funding acquisition, H.A.-T., M.A.H. and M.A.; Investigation, A.O.; Methodology, L.D.; Project administration, M.A.H.; Resources, H.A.-T. and M.A.H.; Software, L.D. and A.O.; Supervision, M.A.H.; Validation, M.A.; Visualization, A.O.; Writing—original draft, H.A.-T. and L.D.; Writing—review and editing, H.A.-T., M.A. and A.O. All authors have read and agreed to the published version of the manuscript.

Funding: This research received no external funding.

Data Availability Statement: The original contributions presented in this study are included in the article, and further inquiries can be directed to the corresponding author.

Conflicts of Interest: The authors declare no conflicts of interest

References

1. Wang, C.; Luo, D.; Deng, Q.; Yang, G. Dynamics analysis and FPGA implementation of discrete memristive cellular neural network with heterogeneous activation functions. *Chaos Solitons Fractals* **2024**, *187*, 115471. [[CrossRef](#)]
2. Li, J.; Wang, C.; Deng, Q. Symmetric multi-double-scroll attractors in Hopfield neural network under pulse controlled memristor. *Nonlinear Dyn.* **2024**, *112*, 14463–14477. [[CrossRef](#)]
3. Kong, X.; Yu, F.; Yao, W.; Cai, S.; Zhang, J.; Lin, H. Memristor-induced hyperchaos, multiscroll and extreme multistability in fractional-order HNN: Image encryption and FPGA implementation. *Neural Netw.* **2024**, *171*, 85–103. [[CrossRef](#)]
4. Deng, Q.; Wang, C.; Sun, Y.; Deng, Z.; Yang, G. Memristive tabu learning neuron generated multi-wing attractor with FPGA implementation and application in encryption. *IEEE Trans. Circuits Syst. I Regul. Pap.* **2024**, *72*, 300–311. [[CrossRef](#)]
5. Qian, K.; Xiao, Y.; Wei, Y.; Liu, D.; Wang, Q.; Feng, W. A robust memristor-enhanced polynomial hyper-chaotic map and its multi-channel image encryption application. *Micromachines* **2023**, *14*, 2090. [[CrossRef](#)] [[PubMed](#)]
6. Vignesh, D.; Banerjee, S. Dynamical analysis of a fractional discrete-time vocal system. *Nonlinear Dyn.* **2023**, *111*, 4501–4515. [[CrossRef](#)]
7. Feng, W.; Wang, Q.; Liu, H.; Ren, Y.; Zhang, J.; Zhang, S.; Qian, K.; Wen, H. Exploiting newly designed fractional-order 3D Lorenz chaotic system and 2D discrete polynomial hyper-chaotic map for high-performance multi-image encryption. *Fractal Fract.* **2023**, *7*, 887. [[CrossRef](#)]
8. Arora, S.; Mathur, T.; Agarwal, S.; Tiwari, K.; Gupta, P. Applications of fractional calculus in computer vision: A survey. *Neurocomputing* **2022**, *489*, 407–428. [[CrossRef](#)]
9. Abdeljawad, T.; Sher, M.; Shah, K.; Sarwar, M.; Amacha, I.; Alqudah, M.; Al-Jaser, A. Analysis of a class of fractal hybrid fractional differential equation with application to a biological model. *Sci. Rep.* **2024**, *14*, 18937. [[CrossRef](#)] [[PubMed](#)]
10. Sharafian, A.; Ali, A.; Ullah, I.; Khalifa, T.R.; Bai, X.; Qiu, L. Fuzzy Adaptive Control for Consensus Tracking in Multiagent Systems with Incommensurate Fractional-Order Dynamics: Application to Power Systems. *Inf. Sci.* **2024**, *689*, 121455. [[CrossRef](#)]
11. Hamadneh, T.; Abbas, A.; Al-Tarawneh, H.; Gharib, G.M.; Salameh, W.M.M.; Al Soudi, M.S.; Ouannas, A. On chaos and complexity analysis for a new sine-based memristor map with commensurate and incommensurate fractional orders. *Mathematics* **2023**, *11*, 4308. [[CrossRef](#)]
12. Gholamin, P.; Sheikhani, A.R.; Ansari, A. Stabilization of a new commensurate/incommensurate fractional order chaotic system. *Asian J. Control* **2021**, *23*, 882–893. [[CrossRef](#)]
13. Vignesh, D.; He, S.; Fataf, N.A.A. Chaotic dynamics of fractional difference magnetic levitation model with application to image encryption. *Eur. Phys. J. Spec. Top.* **2023**, *232*, 2675–2691. [[CrossRef](#)]
14. Ahmadi, A.; Parthasarathy, S.; Pal, N.; Rajagopal, K.; Jafari, S.; Tlelo-Cuautle, E. Extreme multistability and extreme events in a novel chaotic circuit with hidden attractors. *Int. J. Bifurc. Chaos* **2022**, *33*, 2330016. [[CrossRef](#)]

15. Peng, Y.; Lan, Z.; Li, W.; Li, Y.; Peng, J. Modeling different discrete memristive sine maps and its parameter identification. *Eur. Phys. J. Spec. Top.* **2022**, *231*, 3187–3196. [[CrossRef](#)]
16. Wu, X.; Fu, L.; He, S.; Yao, Z.; Wang, H.; Han, J. Hidden attractors in a new fractional-order Chua system with arctan nonlinearity and its DSP implementation. *Results Phys.* **2023**, *52*, 106866. [[CrossRef](#)]
17. Kumar, S.; Matouk, A.E.; Chaudhary, H.; Kant, S. Control and synchronization of fractional-order chaotic satellite systems using feedback and adaptive control techniques. *Int. J. Adapt. Control. Signal Process.* **2021**, *35*, 484–497. [[CrossRef](#)]
18. Li, C.; Yi, C.; Li, Y.; Mitro, S.; Wang, Z. Offset boosting in a discrete system. *Chaos Interdiscip. J. Nonlinear Sci.* **2024**, *34*, 031102. [[CrossRef](#)]
19. Hamadneh, T.; Ahmed, S.B.; Al-Tarawneh, H.; Alsayyed, O.; Gharib, G.M.; Al Soudi, M.S.; Abbes, A.; Ouannas, A.; The new four-dimensional fractional chaotic map with constant and variable-order: Chaos, control and synchronization. *Mathematics* **2023**, *11*, 4332. [[CrossRef](#)]
20. Balootaki, M.A.; Rahmani, H.; Moeinkhah, H.; Mohammadzadeh, A. On the synchronization and stabilization of fractional-order chaotic systems: Recent advances and future perspectives. *Phys. A Stat. Mech. Its Appl.* **2020**, *551*, 124203. [[CrossRef](#)]
21. Zaqueros-Martinez, J.; Rodriguez-Gomez, G.; Tlelo-Cuautle, E.; Orihuela-Espina, F. Fuzzy synchronization of chaotic systems with hidden attractors. *Entropy* **2023**, *25*, 495. [[CrossRef](#)]
22. Elaskar, S. Symmetry in Nonlinear Dynamics and Chaos. *Symmetry* **2022**, *15*, 102. [[CrossRef](#)]
23. Wang, R.; Li, C.; Kong, S.; Jiang, Y.; Lei, T. A 3D memristive chaotic system with conditional symmetry. *Chaos Solitons Fractals* **2022**, *158*, 111992. [[CrossRef](#)]
24. Karimov, T.; Rybin, V.; Kolev, G.; Rodionova, E.; Butusov, D. Chaotic communication system with symmetry-based modulation. *Appl. Sci.* **2021**, *11*, 3698. [[CrossRef](#)]
25. Elbadri, M.; Abdoon, M.A.; Berir, M.; Almutairi, D.K. A symmetry chaotic model with fractional derivative order via two different methods. *Symmetry* **2023**, *15*, 1151. [[CrossRef](#)]
26. Xu, Q.; Cheng, S.; Ju, Z.; Chen, M.; Wu, H. Asymmetric coexisting bifurcations and multi-stability in an asymmetric memristive diode-bridge-based jerk circuit. *Chin. J. Phys.* **2021**, *70*, 69–81. [[CrossRef](#)]
27. Lin, H.; Wang, C.; Sun, J.; Zhang, X.; Sun, Y.; Iu, H.H. Memristor-coupled asymmetric neural networks: Bionic modeling, chaotic dynamics analysis and encryption application. *Chaos Solitons Fractals* **2023**, *166*, 112905. [[CrossRef](#)]
28. Al-Taani, H.; Abu Hammad, M.M.; Abudayah, M.; Diabi, L.; Ouannas, A. Asymmetry and Symmetry in New Three-Dimensional Chaotic Map with Commensurate and Incommensurate Fractional Orders. *Symmetry* **2024**, *16*, 1447. [[CrossRef](#)]
29. Baione, F.; Biancalana, D.; De Angelis, P. An application of Sigmoid and Double-Sigmoid functions for dynamic policyholder behaviour. *Decis. Econ. Financ.* **2021**, *44*, 5–22. [[CrossRef](#)]
30. Mfungo, D.E.; Fu, X.; Wang, X.; Xian, Y. Enhancing image encryption with the Kronecker Xor product, the Hill Cipher, and the Sigmoid Logistic Map. *Appl. Sci.* **2023**, *13*, 4034. [[CrossRef](#)]
31. Martinelli, C.; Coraddu, A.; Cammarano, A. Approximating piecewise nonlinearities in dynamic systems with sigmoid functions: Advantages and limitations. *Nonlinear Dyn.* **2023**, *111*, 8545–8569. [[CrossRef](#)]
32. Pratiwi, H.; Windarto, A.P.; Susliansyah, S.; Aria, R.R.; Susilowati, S.; Rahayu, L.K.; Fitriani, Y.; Merdekawati, A.; Rahadjeng, I.R. Sigmoid activation function in selecting the best model of artificial neural networks. *J. Phys. Conf. Ser.* **2020**, *1471*, 012010. [[CrossRef](#)]
33. Jiang, H.G.; Jia, M.M. Chaos control for multi-scroll chaotic attractors generated by introducing a bipolar sigmoid function series. *Indian J. Phys.* **2020**, *94*, 851–861. [[CrossRef](#)]
34. Abdeljawad, T. On Riemann and Caputo fractional differences. *Comput. Math. Appl.* **2011**, *62*, 1602–1611. [[CrossRef](#)]
35. Atici, F.M.; Eloe, P. Discrete fractional calculus with the nabla operator. *Electron. J. Qual. Theory Differ. Equ.* [*Electron. Only*] **2009**, *62*, 1–12. [[CrossRef](#)]
36. Wu, G.C.; Baleanu, D. Discrete fractional logistic map and its chaos. *Nonlinear Dyn.* **2014**, *75*, 283–287. [[CrossRef](#)]
37. Shatnawi, M.T.; Djenina, N.; Ouannas, A.; Batiha, I.M.; Grassi, G. Novel convenient conditions for the stability of nonlinear incommensurate fractional-order difference systems. *Alex. Eng. J.* **2022**, *61*, 1655–1663. [[CrossRef](#)]
38. Bao, H.; Hua, Z.; Li, H.; Chen, M.; Bao, B. Discrete memristor hyperchaotic maps. *IEEE Trans. Circuits Syst. I Regul. Pap.* **2021**, *68*, 4534–4544 [[CrossRef](#)]
39. Thoai, V.P.; Pham, V.T.; Grassi, G.; Momani, S. Assessing sigmoidal function on memristive maps. *Heliyon* **2024**, *10*, e27781. [[CrossRef](#)] [[PubMed](#)]
40. Anastassiou, G.A. General Multiple Sigmoid Functions Relied Complex Valued Multivariate Trigonometric and Hyperbolic Neural Network Approximations. 2023. Available online: <https://rgmia.org/papers/v26/v26a43.pdf> (accessed on 1 December 2024).
41. Wu, G.C.; Baleanu, D. Jacobian matrix algorithm for Lyapunov exponents of the discrete fractional maps. *Commun. Nonlinear Sci. Numer. Simul.* **2015**, *22*, 95–100. [[CrossRef](#)]
42. Gottwald, G.A.; Melbourne, I. The 0-1 test for chaos: A review. In *Chaos Detection and Predictability*; Springer: Berlin/Heidelberg, Germany, 2016; pp. 221–247.

43. Richman, J.S.; Moorman, J.R. Physiological time-series analysis using approximate entropy and sample entropy. *Am. J. Physiol.-Heart Circ. Physiol.* **2000**, *278*, H2039–H2049. [[CrossRef](#)]
44. Li, Y.; Wang, X.; Liu, Z.; Liang, X.; Si, S. The entropy algorithm and its variants in the fault diagnosis of rotating machinery: A review. *IEEE Access* **2018**, *6*, 66723–66741. [[CrossRef](#)]
45. Shen, E.-H.; Cai, Z.-J.; Gu, F.-J. Mathematical foundation of a new complexity measure. *Appl. Math. Mech.* **2005**, *26*, 1188–1196.

Disclaimer/Publisher’s Note: The statements, opinions and data contained in all publications are solely those of the individual author(s) and contributor(s) and not of MDPI and/or the editor(s). MDPI and/or the editor(s) disclaim responsibility for any injury to people or property resulting from any ideas, methods, instructions or products referred to in the content.